Performance Enhancement of a Thermally Activated Cooling System Using Microchannel Heat Exchangers

Hailei Wang* and Richard B. Peterson

School of Mechanical, Industrial, & Manufacturing Engineering

204 Rogers Hall, Oregon State University

Corvallis, OR 97331, USA

* Corresponding Author

Phone: 541-713-1354, Fax: 541-758-9320, Email: wanghai@engr.orst.edu

Abstract

In the current study a thermally activated cooling system that combines an ORC system with a vapor compression cooling cycle was developed and tested under laboratory conditions. This combined system can utilize waste heat or other thermal sources such as solar and geothermal to generate power and cooling. Hot oil with temperature up to 200 °C was used as the simulated heat source for its convenience. Microchannel heat exchangers were used throughout the system in order to meet the performance, size and weight challenges. Two conventional plate heat exchangers for the boiler and recuperator were also tested inside the system for comparison purposes. Compared to the plate boiler and recuperator, the integrated microchannel boiler/recuperator displayed significant improvement of the heat transfer effectiveness over the range of mass flow rates examined which translates to higher conversion efficiency and overall COP. A simplified model, used to design the microchannel recuperator, ignores the entrance and conjugate heat transfer effects, but it appears to match well the trend of measured average heat transfer coefficients for all cases tested. After taking into account the channel side walls, the measured values of the average heat transfer coefficient agree also with the predicted one. Because of this relatively conservative design approach, the actual heat transfer effectiveness for the recuperator was significantly higher than the designed value of 85%. With the integrated microchannel boiler/recuperator, this thermally activated cooling system was able to achieve over 5 kW of cooling and approached an overall COP of 0.8 under laboratory conditions.

Keywords: microchannel, heat exchanger, performance enhancement, efficiency, organic Rankine cycle (ORC), cooling, waste heat recovery

Nomenclatures

A heat transfer area (m^2)

C_{min} minimum heat capacity (W/C)

C_{max} maximum heat capacity (W/C)

COP coefficient of performance

D_h	hydraulic diameter (m)
E	exergy (W)
f	friction factor
Gz	Graetz number
h	convective heat transfer coefficient (W/m^2-C)
k	thermal conductivity (W/m-C)
m	mass flow rate (kg/s)
M	Maranzana number
NTU	number of transfer unit
Nu	Nusselt number
Pr	Prandtl number
Q	heat (W)
Re	Reynolds number
t	wall thickness (m)
T_0	temperature at dead state (°C)
U	overall heat transfer coefficient (W/m^2-C)
W	work (W)
ε	heat transfer effectiveness
η	efficiency

Subscripts

air	air
ave	average
BI	*boiler inlet*
boi	boiler
c	cooling cycle
com	compressor

con	condenser
d	*destruction*
D	*diameter*
EI	*expander inlet*
EO	*expander outlet*
eva	evaporator
exp	expander
f	fluid
h	hydraulic
l	liquid
OI	*oil inlet*
oil	oil
OO	*oil outlet*
p	power *cycle*
PCI	*power condenser inlet*
PCO	*power condenser outlet*
PI	*pump inlet*
PO	*pump outlet*
recup	recuperator
s	system
v	vapor
w	wall

1   Introduction

As energy demand continues to grow worldwide, the concept of diversifying energy sources and reducing our dependency on fossil fuels has been widely accepted. Progress in this effort can be along two different paths. On the one hand, renewable energy sources such as solar, wind and geothermal are playing more important roles in the world energy supply. On the other hand, there continues to be significant potential for reducing energy consumption and greenhouse gas emission by improving overall energy efficiency for various energy systems. One route toward satisfying both paths is to develop technology able to recover

waste (or otherwise low-grade if from renewables) heat that would be otherwise rejected to the atmosphere without usage. A good example of that is internal combustion engine. It is well known that internal combustion engines generally operate at 25 to 40 percent conversion efficiency from fuel to power. Consequently there are large amounts of high grade waste thermal energy (350 to 500 °C) rejected to the atmosphere across the entire transportation sector nationwide, which includes light-duty and heavy-duty vehicles. Many mobile power generators, driven by diesel engines, also dissipate significant waste thermal energy during operations. Currently, most of these high-to-medium grade thermal sources exhaust to the environment without further utilization, which presents significant opportunities for waste heat recovery and thus improved overall fuel efficiency. Similarly, many industrial processes are also inefficient and create additional opportunities for waste heat recovery. It has been estimated that industrial low-grade waste heat accounts for more than 50 percent of heat generated [1].

In order to improve overall energy efficiency, waste heat has to be converted into a useful form such as for producing hot water or for space heating. Another option is converting the waste heat into higher grade energy such as power or cooling. One method that has attracted much attention is thermoelectric conversion (TEC) due to its simplicity associated with solid state components. Because of this characteristic, there have been numerous studies on thermoelectric power generation for waste heat recovery. Many of the studies have focused on developing higher efficiency TE materials and optimizing their manufacturing process. Others demonstrate system level integration to utilize these new TE materials. However, the conversion efficiency for most TE modules currently remains low. There has been recent interest in creating hybrid power and cooling systems that can leverage the benefits of TE systems with other power and cooling technologies to provide flexible, robust systems in different applications [2-5].

Another technology which has regained significant interest in recent years due to environmental and economical concerns is the organic Rankine cycle (ORC). It remains a strong candidate for converting low-to-medium grade heat into power due to its technology maturity and relatively high thermal conversion efficiency. In recent years, it has been demonstrated and studied using renewable energy sources such as solar [6-8], geothermal [9,10] and waste heat [11-19] to produce electric power. Besides power generation, another interested application for ORC is water desalination [20-22], where the power generated in an ORC is used to drive a reverse osmosis system to produce fresh water from sea water. In this study, an ORC is used to drive a vapor compression cycle to achieve space cooling. Instead of using power from a diesel generator for the motor/compressor, the vapor compression cooling cycle can be driven by waste heat coming off the engine exhaust flow to provide heat to an ORC. Direct coupling of the output shaft of the ORC to the compressor of the cooling system provides the coupling between these two cycles. Compared to other thermally activated cooling technology, the most prominent being the absorption cycle, the current system provides advantages in terms of overall efficiency and has the flexibility of producing power when cooling is not needed.

2   Microchannel Heat Exchangers

Since Tuckerman and Pease [23] first published their work in 1981, microchannel fluid flow and heat transfer have been studied extensively in the electronics cooling industry over the past three decades. Most of the studies found that classical correlations based on conventional or macro-scale channels still work in microchannels [24-29]. However, some scaling effects such as entrance effects and conjugate heat transfer, often negligible in conventional channels, may now have a significant influence and thus

need to be accounted for [30-32]. Similarly, microchannel heat exchangers offer the same advantages that can significantly increase heat transfer rates at much reduced sizes [33]. It can be considered as one of the enabling technologies for compact or portable energy conversion systems where space is limited and weight is critical for the overall design goals. In addition, the working fluid charge for the system can be reduced significantly, rendering better compliance with the environmental mandates. Microchannel condensers and evaporators [34-37], for example, have been successfully used in the air-conditioning industry due to the advantages mentioned above, especially in mobile air-conditioning units. The hydraulic diameter of the channels in these condensers and evaporators is slightly over 1 mm. In contrast, the size of a microchannel used for electronics cooling is typically less than 200 μm [38].

The fundamental driving factor for using microchannel heat exchangers lies in eq. (1), where Nu is the Nusselt number, h is the convective heat transfer coefficient, D_h is the hydraulic diameter of the microchannels, and k is the thermal conductivity of the fluid. For a fully developed laminar flow with constant heat flux boundary condition, the Nusselt number is a fixed value, 5.33 for rectangular channels with an aspect ratio of 4. As the hydraulic diameter is reduced by an order of magnitude from a few millimeters for conventional tubes to a few hundreds of micrometers for microchannels, the convective heat transfer coefficients can be an order of magnitude larger. This is particularly favorable for gas or vapor flows whose thermal conductivities are typically very low. In addition, the ratio of wet surface-to-volume for microchannel heat exchangers is significantly higher than conventional heat exchangers such as tube-fin and plate. Therefore using microchannel in a heat exchanger application creates a double effect – higher heat transfer coefficients and higher heat transfer areas. One of the concerns of using microchannels is the potentially higher pressure drop associated with smaller flow passage. However this can normally be resolved by a careful design ensuring sufficient cross-sectional flow area. In addition, the flow length inside microchannel heat exchangers are typically much shorter for a given heat duty, which will help reduce overall pressure drop.

$$Nu = \frac{hD_h}{k}$$
(1)

3   System Testing and Components Design

3.1   System level design
The thermally activated cooling system was designed to utilize medium-to-low grade waste heat to generate cooling. Essentially, it combines an ORC with a vapor compression cooling cycle. The cooling capacity under design conditions is 5.3 kW. Figure 1 shows the P&ID diagram of the combined cycle. The ORC working fluid was firstly vaporized in the boiler. The superheated vapor then flows through the scroll expander to produce shaft work (the latest scroll expander performance can be found in [39]). HFC-245fa from Honeywell was selected as the working fluid not only because i t has desirable thermodynamic properties for recovering low-grade waste heat, but also it has zero ODP, low GWP and is non-toxic, non-flammable, and non-corrosive for practical reasons. As a drying working fluid upon expansion, the vapor still contains significant amounts of sensible heat upon exiting the expander. The vapor then enters the recuperator to preheat the fluid going to the boiler. This internal heat recuperation is important for improving cycle efficiency as the required amount of heat at the boiler is reduced and the average heat input temperature is increased. The vapor then enters the power condenser to reject heat to the environment. The slightly subcooled fluid flows into the reservoir and then to the pump where the

pressure is raised. The exiting high pressure fluid goes through the recuperator and enters the boiler to complete the cycle. The cooling side is based on a standard vapor compression cycle. Instead of using an electrical motor to drive the compressor, a refrigeration scroll compressor was modified to directly couplewith the scroll expander through a common shaft (detailed information can be found in [39]). The conversion losses associated with an electrical generator and motor, typically 20 to 40 percent are eliminated. The high pressure vapor after compression goes through the standard condensing and evaporating processes before completing the loop. A 1.5 tons (5.3 kW) thermostatic expansion valve from Sporlan Inc. was selected. The working fluid HFC-134a was used as the refrigerant, as it is found widely in various mobile air-conditioning systems.
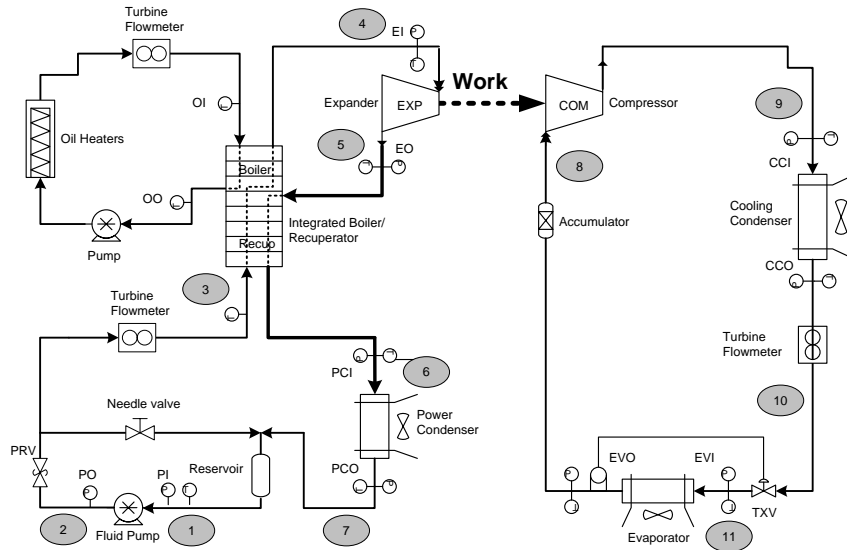

Figure 1: Schematic Flow Diagram for the Heat Activated Cooling System

Figure 2: Combined Cycle Prototype Unit Front View (left) with the Hot Oil Circulator (right).

Figure 3: The Back View of the Combined Cycle Prototype Unit (size: $30 \times 32 \times 34$ inches)

During tests conducted under laboratory conditions, a hot oil circulator was used to simulate the heat source. The combined cycle prototype unit (on the right) and the hot oil circulator (on the left) are shown in Fig. 2. The view is from the front side of the prototype unit, where the evaporator panel was situated. The louver panel in front of the brazed aluminum microchannel (BAM) evaporator protects the air fins and directs the flow. Two impellers were used behind the evaporator to draw air from the center of the front surface; and blow the cooled air out to the room through both the top and bottom slots. The4 axial fans sitting on the top of the unit provided air flow to cool both the power and cooling condensers. They are designed to provide a draw-through system, which means cooling air is pulled through the power and cooling condensers on each side of the unit and exits from the top. A back view of the prototype unit is shown in Fig. 3.

A series laboratory tests were conducted to assess the performance of the prototype unit over a range of conditions. Due to facility limitations, the system has not yet been tested under its design conditions with outdoor condenser air temperature of 48.9 °C and indoor evaporator air temperature of 32 °C. Rather, the system was tested indoors with an air temperature at approximately 22 °C. The typical pressure-enthalpy (P-h) diagrams for the power and cooling cycle are shown in Figs. 4 and 5, respectively. The graphs provide in visual form the cycle conversion performance. As the boiling takes place from state point 3 to point 4 in Fig. 4, the corresponding distance on the horizontal axis (enthalpy) indicates the amount of heat input in the boiler. In contrast, the work generated by the expander is projected on the horizontal axis between state points 4 and 5. The ratio of these two is the conversion efficiency of the power cycle. For a given heat input to the boiler, as the length of the projection on the horizontal axis from point 4 to 5 increases, the better is the energy conversion efficiency. Also, from the second law perspective, less entropy is generated in the process as the slope between state points 4 and 5 decreases. Similarly in Fig. 5, the horizontal distance from state point 11 to point 8 represents the heat absorbed in the evaporator, while the horizontal distance from points 8 to 9 represents the work consumed by the compressor. The ratio of these two quantities visually shows the coefficient of performance (COP) for the cooling cycle.
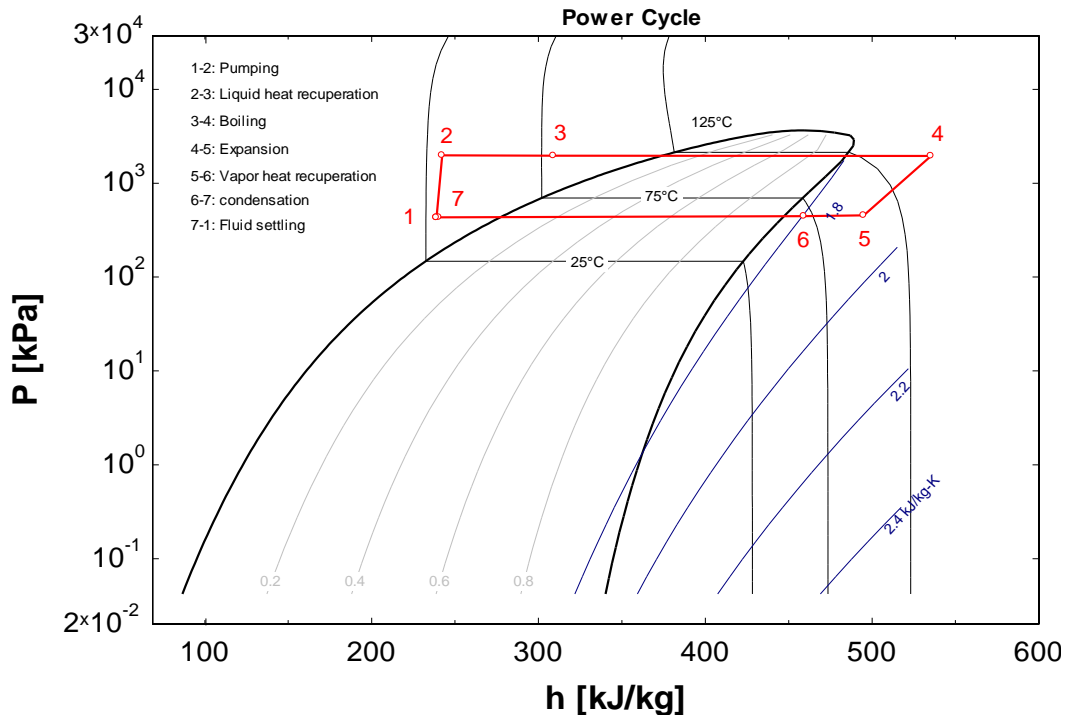
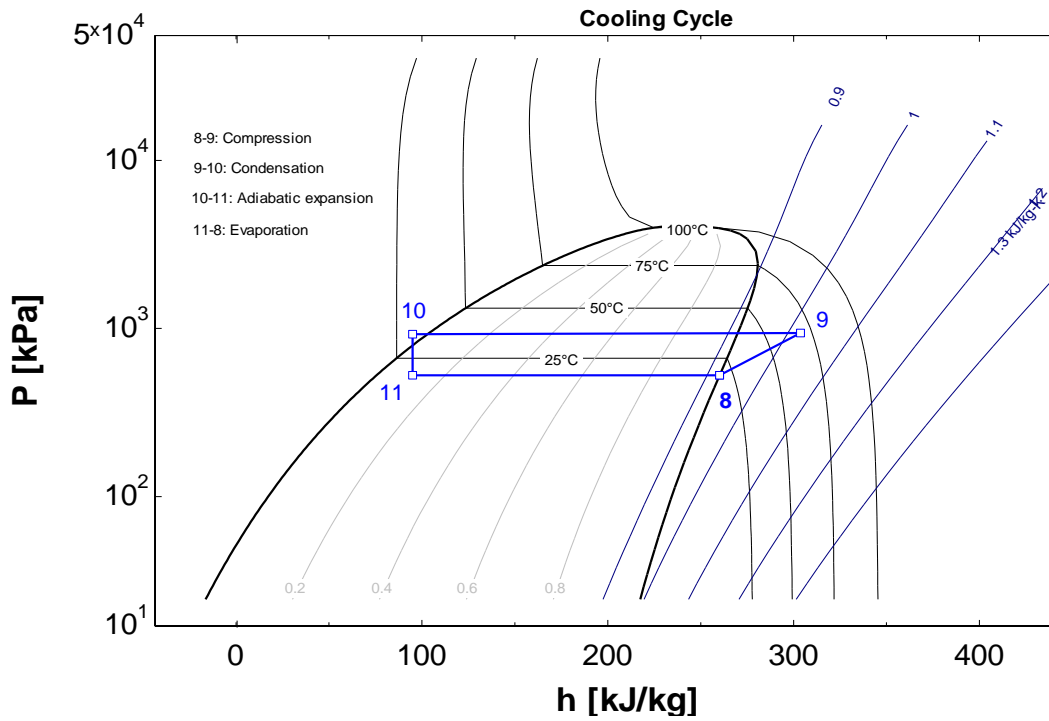Figure 4: The power Cycle Pressure-Enthalpy Diagram

Figure 5: The Cooling Cycle Pressure-Enthalpy Diagram

3.2   Microchannel boiler/recuperator

The current thermally activated cooling system was intended to recover waste heat from diesel generator sets, which typically produce 10 kW of electric power to run communication equipment and an environmental control unit (ECU) or air-conditioning unit. It is anticipated that the fuel consumption by the diesel engine could drop significantly by using waste heat to drive the ECU. Due to the mobile nature of the application, the size and weight of this thermally activated cooling system is specified with the goal of achieving 5.3 kW of cooling at the design conditions. In order to meet the design challenges, all heat transfer components in the combined cycle system were microchannel heat exchangers. An integrated microchannel boiler/recuperator was designed for the ORC side; additionally all the condensers and evaporator were based on brazed aluminum microchannels (BAM). A detailed description of the microchannel recuperator design involving single-phase liquid and vapor flow, is provided as follows.

3.2.1   Design

Although there are many design aspects to be considered, the single most important one is to properly calculate the required heat transfer area. According to the thermodynamic model of the cycle, the recuperator requires an effectiveness of over 85% to achieve the targeted COP. The ε-NTU method was used to calculate the heat transfer rate and area, given that the inlet conditions of the liquid and vapor streams are known. For counter-flow heat exchangers, the effectiveness is

$$\varepsilon = \frac{1 - \exp[-NTU(1 - C_r)]}{1 - C_r \exp[-NTU(1 - C_r)]} \tag{2}$$

where

$$NTU = \frac{UA}{C_{\min}} \tag{3}$$

$$C_r = \frac{C_{\min}}{C_{\max}} = \frac{mCp_v}{mCp_l} \tag{4}$$

For the recuperators, the heat transfer effectiveness is defined as (refer to Fig. (1) for the state points):

$$\varepsilon_{recup} = \frac{Q_{recup}}{Q_{recup,\max}} = \frac{h(P_{EO}, T_{EO}) - h(P_{PCI}, T_{PCI})}{h(P_{EO}, T_{EO}) - h(P_{PCI}, x = 1)} \tag{5}$$

where Q_{recup} represents the enthalpy change of the vapor stream across the recuperators. Although it makes more sense to define Q_{recup} from the liquid side as it represents the amount of heat actually recovered, the current approach eliminates the effect of heat loss which could be significant. This is due to the difference of size and thermal insulation for the microchannel and plate recuperators. $Q_{recup,\max}$ represents the maximum enthalpy change of the vapor stream when it exits from the recuperator as saturation vapor (x = 1). Limiting the exiting fluid to saturated vapor, or not allowing condensation at the recuperator exit, provides a practical advantage because flow distribution at the inlet of the power

condenser could be compromised if two-phase flow emerged from the recuperator and immediately entered the power condenser in the integrated device. Table 1 shows the design parameters associated with the microchannel recuperator.

Table 1: Design parameters for the microchannel recuperator

Effectiveness ε_{recup}	Mass Flow Rate (kg/s)	Vapor Inlet T_{EO} (°C)	Liquid Inlet T_{PO} (°C)	Vapor Inlet P_{EO} (kPa)	Vapor Outlet P_{PCI} (kPa)
85%	0.05	148	68	575	575

In order to calculate the average heat transfer coefficient U shown in eq. (3), the characteristic dimensions of the microchannels were designed first. Table 2 shows those channel dimensions for both the boiler and recuperator sections. Figure 6 provides a schematic channel cross-sectional view of the recuperator section with only one layer of liquid and vapor shim, respectively. Although it contains 41 channels for each individual shim, only two channels are shown here for simple illustration. To make the actual recuperator, this same 2-shim unit repeats 40 times to achieve the design effectiveness. The red dotted lines show the schematics of channel profiles after chemical etching (refer to Fig. 7 for actual channel profiles taken by an optical profilometer).

Table 2: Characteristic channel dimensions for the integrated boiler/recuperator

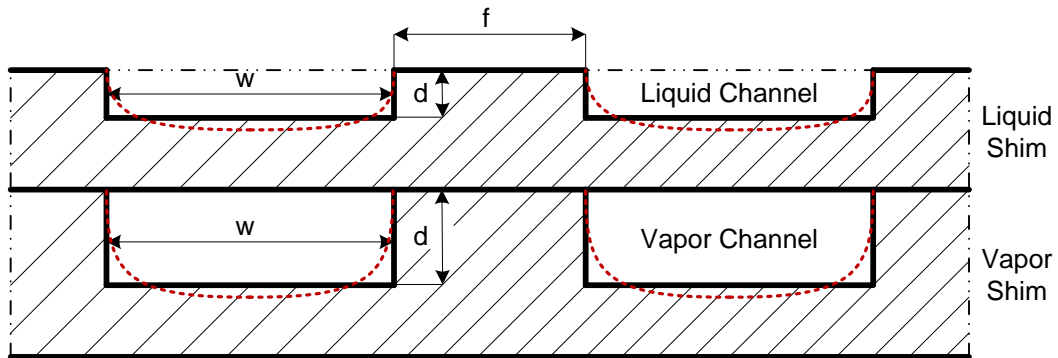|	Boiler – Hot Oil Side	Boiler – Fluid Side	Recuperator – Liquid Side	Recuperator – Vapor Side
Channel Depth, d (µm)	250	380	125	250
Channel Width, w (µm)	1270	1270	1270	1270
Fin Width, f (µm)	890	890	890	890
Hydraulic Diameter (µm)	418	585	228	418

Figure 6: A schematic cross-sectional view of the liquid and vapor channels (recuperator section)

To ensure the performance of the recuperator inside the system, a conservative and simplified design approach was taken based on the following assumptions:

- Fully developed flow (no entrance length effect)

- Constant fluid properties (no change with temperature)

- Constant heat flux boundary condition (no axial conduction, no heat loss)

- Heat transfer area including top and bottom walls of the channel (no side walls)

- Uniform flow distributions between all channels

- Perfect rectangular profile for the channels

Although fluid in the liquid inside microchannels remained laminar flow at all times, fluid inside the vapor channels could turn to turbulent flow in some cases of high flow rates. This is because, for the same mass flow rate, the specific volume for R245fa vapor is almost two orders of magnitude larger than that of R245fa liquid while the viscosity is an order of magnitude smaller. The consequence is much higher Reynolds numbers (Re > 2,300). Given this potential transition to turbulent flow, the Gnielinski correlation [40], shown in eq. (6), was used to predict the Nusselt numbers for the vapor side. The liquid side Nusselt number was based on the well-known value for fully developed laminar flow with constant heat flux, eq. (8).

$$\text{Vapor channels:} \quad Nu_{D,v} = \frac{(f/8)(\mathrm{Re}_{D,v}-1000)\,\mathrm{Pr}}{1+12.7(f/8)^{1/2}(\mathrm{Pr}^{2/3}-1)} \tag{6}$$

where

$$f = (0.79\ln(\mathrm{Re}_{D,v})-1.64)^{-2} \tag{7}$$

$$\text{Liquid channels:} \quad Nu_{D,l} = 6.49 \tag{8}$$

Thus, the calculated overall heat transfer coefficient for the recuperator is

$$\frac{1}{U_{recup}} = \frac{1}{h_v} + \frac{t}{k_w} + \frac{1}{h_l} = \frac{D_{h,v}}{Nu_{D,v}k_v} + \frac{t}{k_w} + \frac{D_{h,l}}{Nu_{D,l}k_l} \tag{9}$$

While the assumptions such as fully developed flow and reduced active heat transfer area lead to a conservative design, assumptions associated with heat loss, axial conduction, boundary conditions and channel profile tend to degrade the performance of the heat exchanger. In order to determine the significance of entrance length effect, the Graetz number defined in Eq. (10) was used. According to Morini [41], the entrance length effect on average Nusselt number can be neglected if the Graetz number is smaller than 10.

$$Gz = \frac{\text{Re Pr } D_h}{L} \tag{10}$$

Because of the high surface area to volume ratio associated with microchannel heat exchangers, heat transfer along channel walls can be significant. A dimensionless Maranzana number [42], defined as

$$M = \frac{k_w}{k_f} \frac{A_w}{A_f} \frac{1}{\text{Re Pr}} \tag{11}$$

was used to determine the significance of axial conduction. It measures the ratio between the axial conduction in the solid walls of the channels and the heat transfer by convection in the fluid. where A_w is the cross-sectional area of the solid walls of the channel and A_f is the area of the surface wetted by the flow. Also in this expression k_w is the thermal conductivity of the channel walls and k_f is the thermal conductivity of the fluid. For the axial conduction in the solids to be neglected, the Maranzana number needs to be smaller than 0.01.

3.2.2   Fabrication

To eliminate the connections between the fluid side of the boiler and the liquid side of the recuperator, and to reduce the heat loss from the device, the microchannel boiler and recuperator were designed to be an integrated unit. As mentioned earlier, the microchannel recuperator contains 40 layers of liquid channel shim and 40 layers of vapor channel shim. Each shim includes 41 channels etched into it. Similarly, the boiler contains 40 layers of fluid shim and 40 layers of oil shim. Both the oil and vapor channels were designed on the same shim, while the liquid channels and fluid channels of the boiler were designed on another shim. The shims were photochemically etched to obtain the designed channel width and depth. Figure 7 shows the vapor channel profiles taken by an optical profilometer indicating curvature at the edges. Then they were plated with a thin layer (a few microns) of nickel phosphor. Besides the shims, there are two end plates used to sandwich the shims. They were surface polished after machining to achieve very smooth finish, which ensured hermetic sealing after the diffusion brazing process.
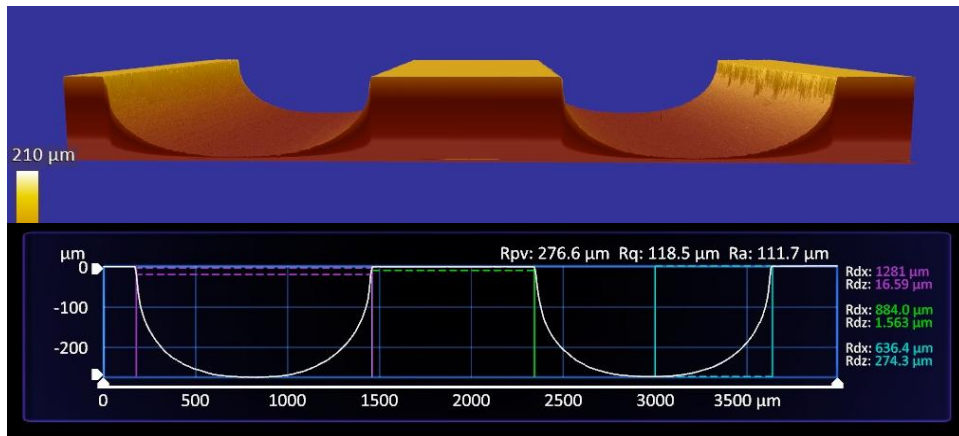

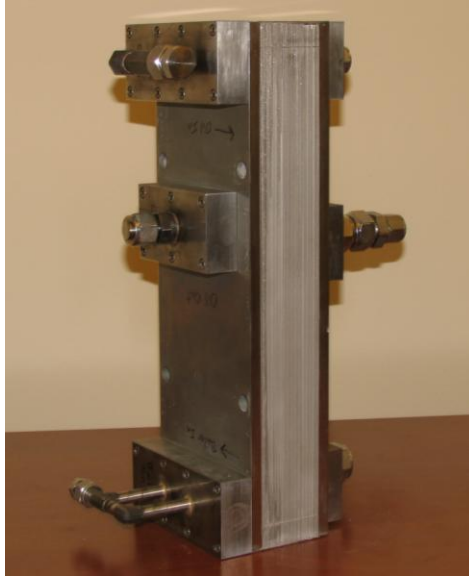Figure 7: Vapor channel profiles taken by an optical profilometer

Figure 8: The integrated microchannel boiler/recuperator (size: $14.75 \times 5.25 \times 2.61$ inches) with attached fittings to the ports

After the shims and end plates were properly registered and assembled, they were diffusion brazed together in a vacuum furnace to form a functional device, which can withstand the design pressure and temperature. All shims and end plates were made of SS 316. The actual picture of the integrated microchannel boiler/recuperator with six header blocks attached is shown in Fig.8. The ratio of its active heat transfer area (2.27 m^2) and volume (0.0033 m^3) is about 690. The six- header-blocks were an approach to avoid post welding, which caused failure of an earlier design. The header blocks were also made of SS 316 and used PTFE o-rings to seal the ports on the end plates. As shown in the picture, the top two ports on the left are hot oil inlet and outlet. The bottom port is where the high pressure liquid enters. The liquid travels upward to recuperate heat from vapor on the other side; and then enters the boiler section (opposite side to the hot oil) where it was fully vaporized and exits from the top right port. In order to achieve high heat transfer effectiveness, both the boiler and recuperator sections were designed in the counter-flow configuration. This implies that the vapor enters the middle port on the right and exits from the bottom port.

3.3 BAM condensers and evaporator

Microchannel condensers and evaporator are used in the current system. They are based on so-called BAM coils, which are constructed of extruded aluminum tubes containing many small rectangular refrigerant ports with hydraulic diameter of 1.22 mm. BAM coil can deliver greater heat exchange capacity than a conventional tube-fin coil in the same space. In other words, a BAM coil can be smaller than a tube-fin coil with the same capacity. In this way, BAM coils are significantly lighter than their traditional counterparts. Besides the small passage for enhanced air side heat transfer, the air side flow length (25.4 mm in the current design) of BAM coils is significantly shorter than that of tube-fin coils. This leads to advantage of using smaller fans and lower fan power requirement. Additional advantages of the BAM coils include their smaller internal volume, which can reduce the refrigerant charge by up to 45% [43-44]. Figure 9 shows a typical microchannel condenser based on BAM coils. It has a two-flow-pass design. The two condensers used in the combined system,

however, have three-flow-pass design. They both have 35 tubes (21 in the first pass, 10 in the second pass and 4 in the third pass). The superheated vapor comes in from the top and subcooled liquid exits from the bottom. Air flows across the panel along the louver fins. The microchannel evaporator, on the other hand, has only one-flow-pass in order to minimize pressure drop. This makes uniform flow distributions harder to achieve, however, particularly with fluid coming in at two-phase. During the system design, the evaporator was oriented such that the two-phase fluid comes in from the bottom and the superheated vapor comes out from the top. During the tests, the temperature profile on the front surface of the evaporator was reasonably uniform, indicating a flow approaching a uniform distribution between the microchannels.

Figure 9: A typical microchannel condensers based on BAM coils

3.4   System testing and uncertainty analysis

A series of tests were conducted under laboratory conditions to evaluate the performance of the prototype unit at both the system and component levels. The collected pressure, temperature, and flow data were used to determine the thermodynamic properties of the working fluid such as enthalpy and entropy at each individual measurement point. These quantities were then used to calculate quantities of interest such as heat transfer rates, coefficients of performance, effectiveness and thermal efficiencies. During testing, many operational parameters were adjusted to observe the responses of the system as well as individual components, and then to optimize the parameters to achieve the performance targets; i.e. a cooling capacity of 5.3 kW and overall system COP (see eq. (16)) of 0.6. In the ORC power side, the parameters include fluid charge amount, mass flow rate, superheat, expander inlet and outlet pressures, condenser fan speed, hot oil inlet temperature and flow rate. In the vapor compression cooling side, the parameters also include fluid charge amount, thermostatic expansion valve settings and condenser fan speed. In the current study, four test cases were presented for each complete system (one system has the microchannel boiler/recuperator; one system has the plate boiler and recuperator). The only active parameter changed for all those cases was mass flow rate by adjusting pump speed, although it also affected the expander inlet and outlet pressures to some degree. In Table 3, values of the most relevant operating parameters associated with those test cases are presented.

Table 3: The relevant operation conditions for each case

System	Parameters	Case 1	Case 2	Case 3	Case 4
Microchannel Boiler and Recuperator	R245fa Mass Flow Rate (kg/s)	0.045	0.038	0.032	0.026
	Vapor Side Reynolds no.	2,758	2,308	1,956	1,604
	Recuperator Liquid Inlet T (°C)	28.5	26.5	25.5	24.6
	Recuperator Vapor Inlet T (°C)	154.9	155.3	153.9	151.1
	Boiler Fluid Outlet T (°C)	193.8	195.0	195.7	195.5
	Expander Inlet P (kPa)	2,164	1,992	1,873	1,749
	Expander Outlet P (kPa)	452	399	358	323
	Oil Inlet T (°C)	198.8	198.4	198.4	197.9
	Oil Flow Rate (LPM)	16.5	16.5	16.5	16.5
Plate Boiler and Recuperator	R245fa Mass Flow Rate (kg/s)	0.037	0.032	0.028	0.025
	Vapor Side Reynolds no.	-	-	-	-
	Recuperator Liquid Inlet T (°C)	26.5	25.7	25.4	25.1
	Recuperator Vapor Inlet T (°C)	141.8	139.6	137.1	137.1
	Boiler Fluid Outlet T (°C)	147.3	145.4	140.0	137.1
	Expander Inlet P (kPa)	1,701	1,589	1,478	1,406
	Expander Outlet P (kPa)	422	405	381	354
	Oil Inlet T (°C)	188.0	188.4	188.5	188.4
	Oil Flow Rate (LPM)	13.7	13.7	13.7	13.7

All temperatures were measured with type K thermocouples made of special limits of error material, which have an uncertainty of ± 1.1 °C or 0.4% of measurement between 0 and 1250 °C. All pressure transducers with inherent 0.25% accuracy were calibrated against a digital pressure gauge with an accuracy of ±0.05% (of full scale range), or ±1.7 kPa. The mass flow rates for both the power and cooling sides were measured by turbine flow meters (AW Company, model TRG-11.300-5) with an accuracy of ±1% of the actual measured flow. The expander power output was measured by a Futek torque sensor (model TRS 605) with rated torque capacity of 10 N-m. It had an accuracy of ±0.3% of the full scale range, or ±0.03 N-m. The uncertainty analysis was focused on the bias errors introduced by the

instruments, as the random errors during the experiments were minimal and averaged out. According to the theory of error propagation, the root-sum-square method was used to combine individual errors. The resulting maximum uncertainties for the quantities of interest are listed in Table 4.

Table 4: Uncertainties for Interested Parameters

Parameter	ε_{recp}	Q_{recup}	U_{recup}	η_p	$\eta_{p,II}$
Uncertainty	2.8%	3.0%	5.0%	3.3%	3.3%

4   Results and Discussion

4.1   *Components performance verification*

In this section, the measured performance of the recuperator and boiler is presented in comparison with the designed values. This approach will also provide an assessment on how close the simplified model matches the experimental data. As shown in Fig. 10, the calculated Graetz and Maranzana numbers for the four test cases are all within the range of $Gz < 10$ and $M < 0.01$, which indicate both entrance length and axial conduction effects can be neglected. This observation to some degree validates the assumptions used in the simplified model. However, the increasing trend of the average heat transfer coefficients with mass flow rate, as shown in Fig. 11 for the four test cases, shows possible effects of the entrance length. This is because, as Reynolds number increases with flow rate, the portion of the entrance length over the entire channel length increases too. This trend also shows up in the Graetz number plot in Fig. 10. Another consideration affecting the Graetz number is the increasing trend of U with mass flow rate; this leads to possible transition-turbulent flow in the vapor channels, however, this transition is captured in the model.

As also shown in Fig. 11, the measured average heat transfer coefficients based on the designed heat transfer area (channel side walls not accounted) are proportionally higher than the predicted ones, which may indicate the actual heat transfer areas were indeed under-estimated. It is very likely a significant amount of channel side walls or fin areas also attributed to the heat transfer, which should be accounted for in the design. Thus, a modified version of the measured average heat transfer coefficients, including the effects of channel side walls, is also plotted for comparison purpose. The predicted ones based on the simplified model are now much closer to the modified ones. The slight divergences at both low and high mass flow rates are likely due to the limitation of the Gnielinski correlation used in the design model. As more test data becomes available, the design model can be modified to closely reflect the flow regimes. Although the design approach is rather conservative from the component point of view, it did serve the purpose of ensuring system performance.
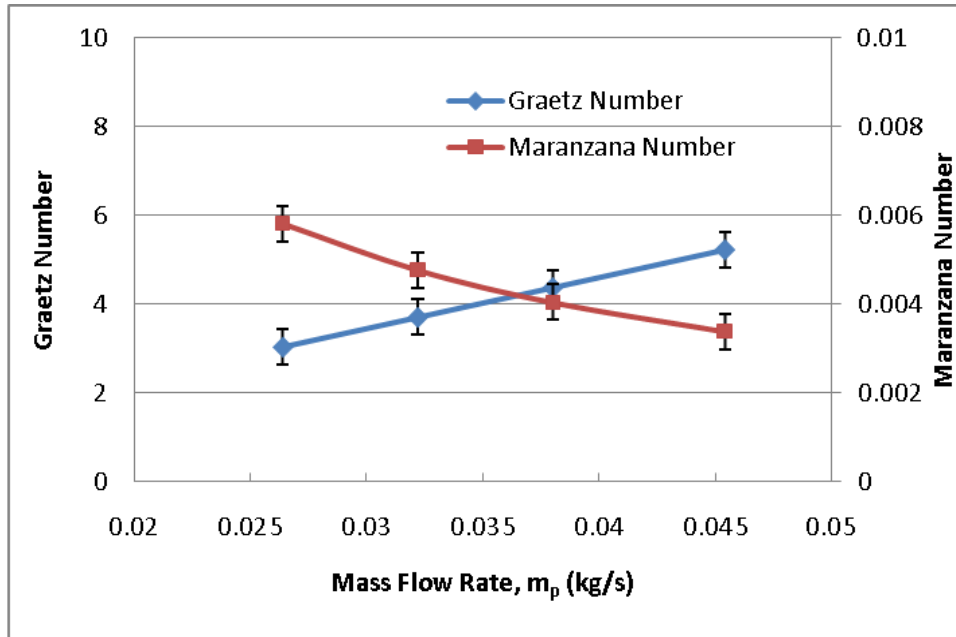
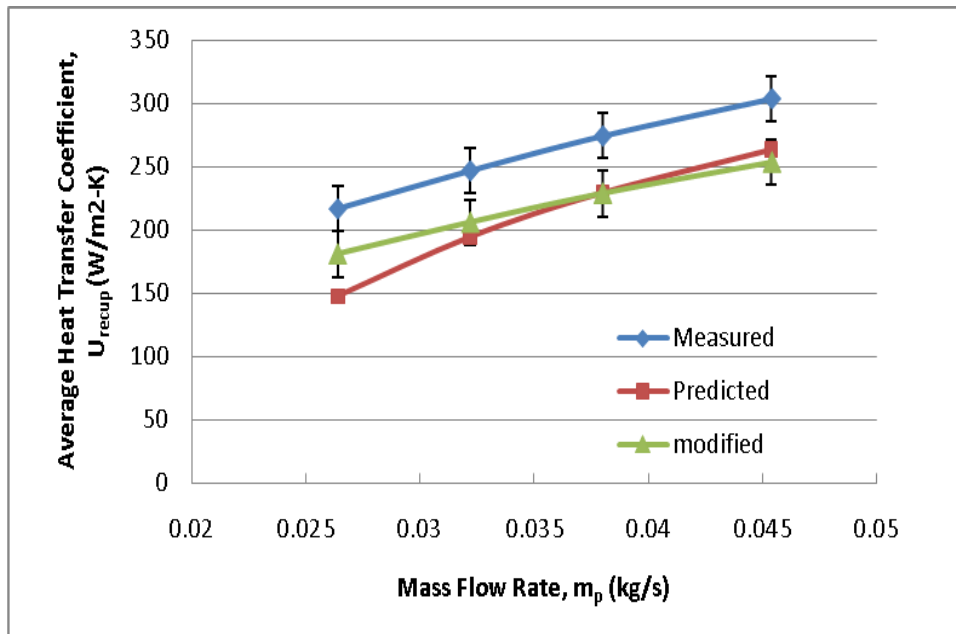Figure 10: The calculated dimensionless numbers for the four test cases

Figure 11: Comparison of measured and model predicted average heat transfer coefficient

Two separate brazed plate heat exchangers (one was made by GEA PHE with model number of FP 5×12-20 and the other was made by ITT Standard with model number of BP 410-30) were used in place of the integrated microchannel boiler/recuperator. It provided an opportunity to establish a baseline performance case, which was compared to the microchannel based integrated unit. Although the weight of the integrated microchannel boiler/recuperator is comparable with that of the combined brazed plate boiler and recuperator due to excess amount of metal around the device perimeters, the size of the integrated microchannel boiler/recuperator is significantly smaller (see Fig. 8 for the dimensions). It took only about

half the space that the plate heat exchangers occupied, without taking into account the tubing connections between the plate boiler and recuperator. In addition, the working fluid charge was reduced by a factor of two for the system using microchannel boiler/recuperator, which again is a significant advantage from the environmental standpoint.

Figure 12 presents the direct comparisons of the microchannel and plate recuperators over a range of mass flow rate. As shown on the left vertical axis, the heat transfer effectiveness of the microchannel recuperator is 15 to 20 percent higher. From the figure, the effectiveness for the microchannel recuperator is in the 98 to 99% range which reflects how the effectiveness was defined in eq. (5). Its practical advantage was also described in the design section. The equation limits the available heat for recuperation after expansion to only sensible heat in the vapor stream, which means the vapor exiting the recuperator at saturation will approach an effectiveness of 100%. Although the effectiveness for the microchannel remained relatively unchanged with the flow rate, there is a clear trend for the plate recuperator that its effectiveness slowly increases with the flow rate. This again indicates the possible entrance length and transition-turbulent effects shown in Fig. 11, resulting in increasing trend of heat transfer coefficient with flow. Besides, the remaining high temperature differences between the liquid and vapor for the plate recuperator helped improving the effectiveness more noticeably.
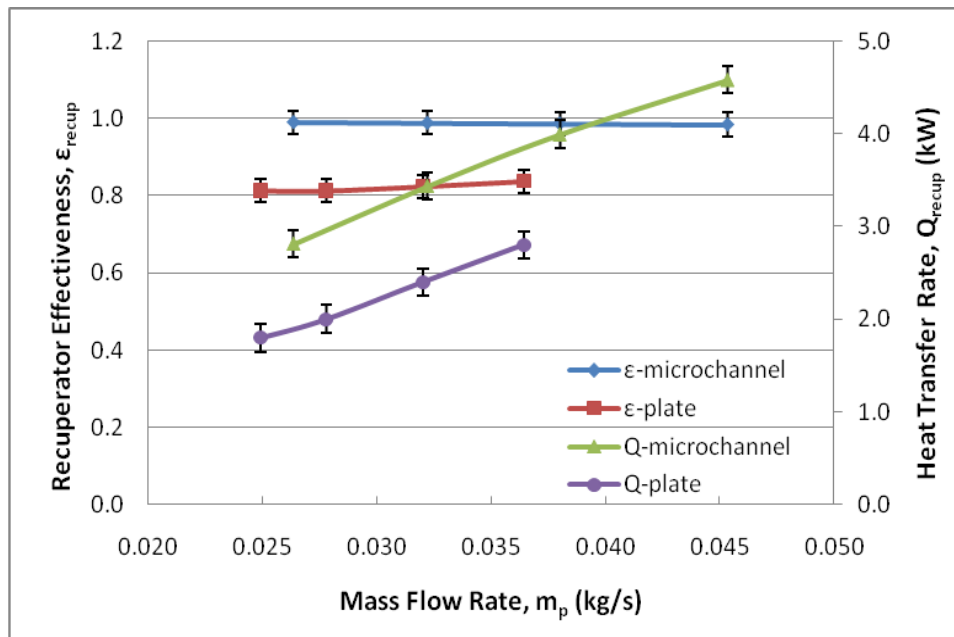

Figure 12: Experimental data to compare the microchannel and plate recuperators

The right vertical axis shows the measured amount of heat that was transferred from the vapor side to the liquid side, assuming no heat loss to the surrounding. In reality, the heat that was recuperated to the liquid side would be slightly lower due to heat loss, even though the components were well insulated. As indicated in the plots, more heat was transferred in the microchannel recuperator for all mass flow rates tested. This is in good agreement with the effectiveness plots. For the mass flow rate of 0.045 kg/s, the amount of heat recovered from the vapor stream was 4.6 kW, which is equal to approximately 42% of the heat supplied to the boiler. This means, if there were no heat recuperation, 42% more heat would be needed in the boiler to maintain the same amount of power output by the ORC. According to the plots, as

the mass flow rate increases more heat can be transferred. The heat transfer enhancement for the microchannel recuperator did come with a penalty, however. As shown in Fig. 13, the vapor side of the microchannel recuperator experienced significantly higher pressure drop than the plate counterpart. This could significantly compromise the rationale of using microchannel heat exchanger with consequence of degrading the power output by the ORC, thus reducing the cooling capacity. One way to mitigate the higher pressure drop is to increase the flow cross-sectional area for the microchannel design, which can be achieved by reducing fin width between channels, increasing channel aspect ratio, increasing the channel layers while reducing channel length, or combination of all these. According to Table 2, there is sizable design space to optimize the dimensions in order to minimize pressure drop.
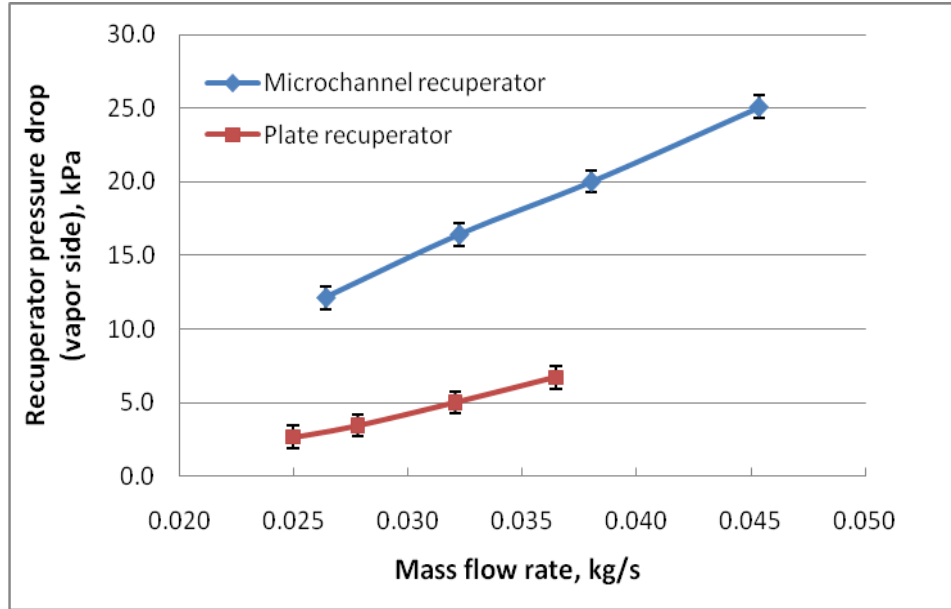

Figure 13: Vapor pressure drops comparison between microchannel and plate recuperators

Similarly, the definition of heat transfer effectiveness for the boiler is (refer to Fig. (1) for the state points):

$$\varepsilon_{boi} = \frac{Q_{boi}}{Q_{boi,\max}} = \frac{h(P_{EI},T_{EI}) - h(P_{BI},T_{BI})}{h(P_{EI},T_{OI}) - h(P_{BI},T_{BI})} \tag{12}$$

where Q_{boi} represents the enthalpy change of the fluid across the boiler and $Q_{boi,\max}$ represents the enthalpy change of the fluid if it exits from the boiler at the temperature of the incoming hot oil. The effectiveness and the amount of superheat achieved for both the microchannel and plate boilers are plotted in Fig.14. The data shows a clear difference between conventional plate and microchannel heat exchangers. For a range of mass flow rates tested, the heat transfer effectiveness of the microchannel boiler, as shown on the left vertical axis, is more than 30 percent higher. Correspondingly, the amount of superheat almost triples as shown in the right vertical axis. This again justifies the advantages of using microchannel heat exchangers, particularly for applications where a fluid's superheated vapor has an inherently poor heat transfer coefficient.
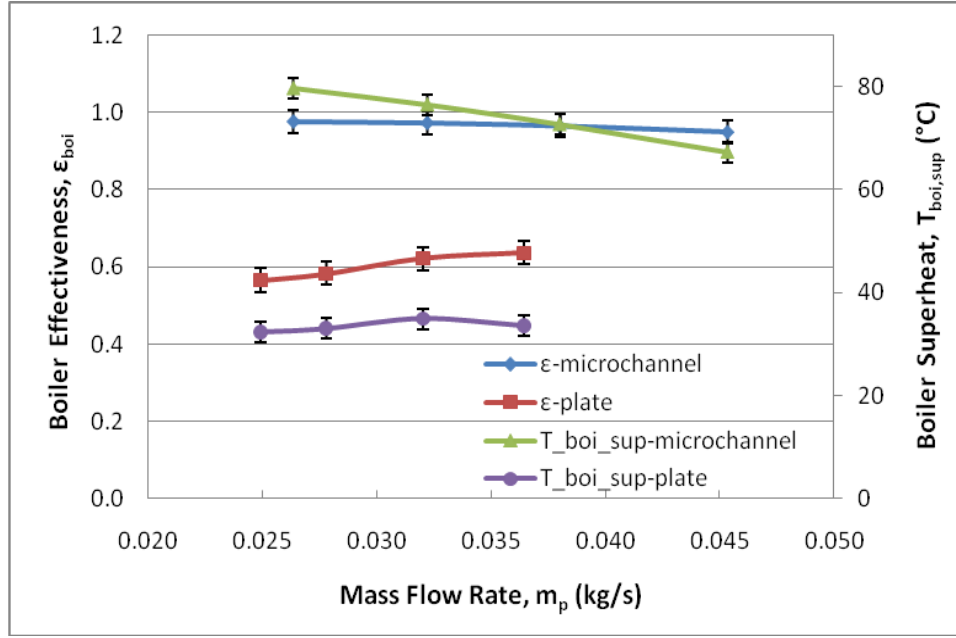
Figure 14: Experimental data to compare the microchannel and plate boilers

4.2 Impact on system performance

In the context of overall system performance, it is important to understand the impact of higher boiler and recuperator heat transfer on the overall system operation besides just the size and weight advantages. Engineering Equation Solver (EES) was used to model the overall system, where the fundamental equations of state based on Helmholtz energy were used to calculate the thermodynamic properties such as enthalpy and entropy at each cycle state point. Below are equations used to define the ORC efficiencies and overall system COPs.

ORC 1st Law efficiency (conversion efficiency):

$$\eta_p = \frac{W_{exp}}{Q_{boi}} \tag{13}$$

Cooling Cycle COP:

$$COP_c = \frac{Q_{eva}}{W_{com}} \tag{14}$$

Assuming the compressor power input equals the expander power output,

$$W_{com} = W_{exp} \tag{15}$$

Overall system COP based on heat activation:

$$COP_s = \frac{Q_{eva}}{Q_{boi}} \tag{16}$$

ORC 2nd law efficiency (Carnot efficiency):

$$\eta_{p,II} = \frac{\eta_p}{\eta_{Carnot}} \tag{17}$$

Where the Carnot efficiency is calculated based on the averaged cooling air temperature for the condenser and averaged heating oil temperature for the boiler. In this case, it is a fixed value given by:

$$\text{Carnot efficiency:} \qquad \eta_{Carnot} = 1 - \frac{T_{air,ave}}{T_{oil,ave}} \qquad (18)$$

As shown in Fig. 14, the amount of superheat for the fluid coming out of the microchannel boiler is significantly higher than that for the plate boiler. This impact on system level performance is shown in Fig. 15, where ORC efficiencies and system COP are plotted against the amount of superheat after the boiler. The left vertical axis shows the 1st law efficiency, while the 2nd law efficiency and system COP are shown on the right vertical axis.
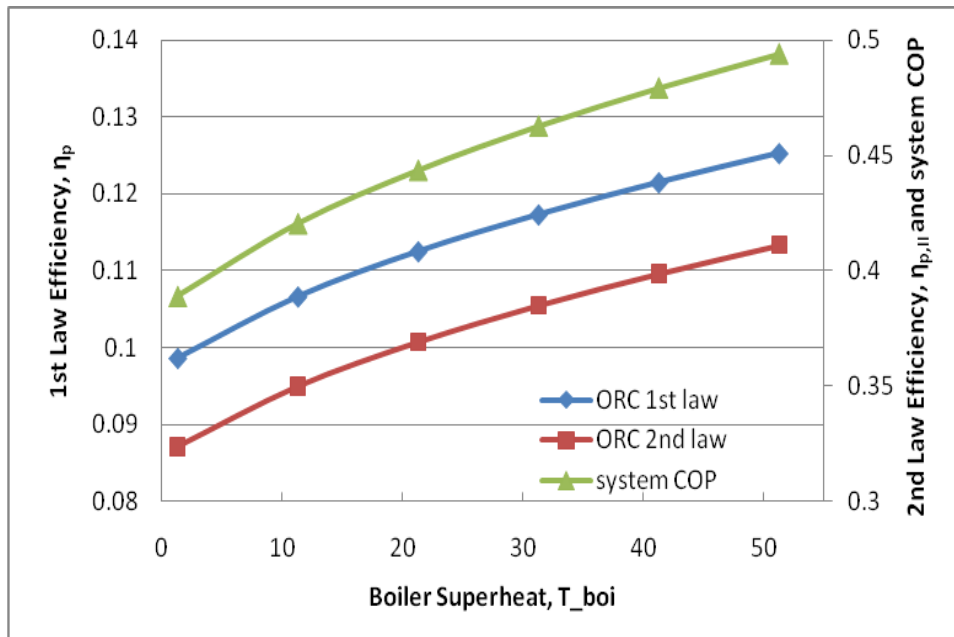

Figure 15: Model data to show the effect of boiler superheat on cycle performance (the plate boiler superheat = 22 °C while the microchannel boiler superheat > 65 °C)

It is clear that higher boiler superheat as the result of improved heat transfer effectiveness has a very positive impact on system performance, from both 1st and 2nd law standpoints. A higher averaged heat input temperature to the fluid in the boiler was observed resulting in enhanced conversion efficiency. The enhancement of ORC efficiency also translates to the increase of the overall system COP. At the same time, there was a closer matched temperature profile between the working fluid and heating oil (see Figs. 16 and 17), particularly in the superheat section of the boiler. This led to higher Carnot efficiency due to less exergy destruction in the microchannel boiler.
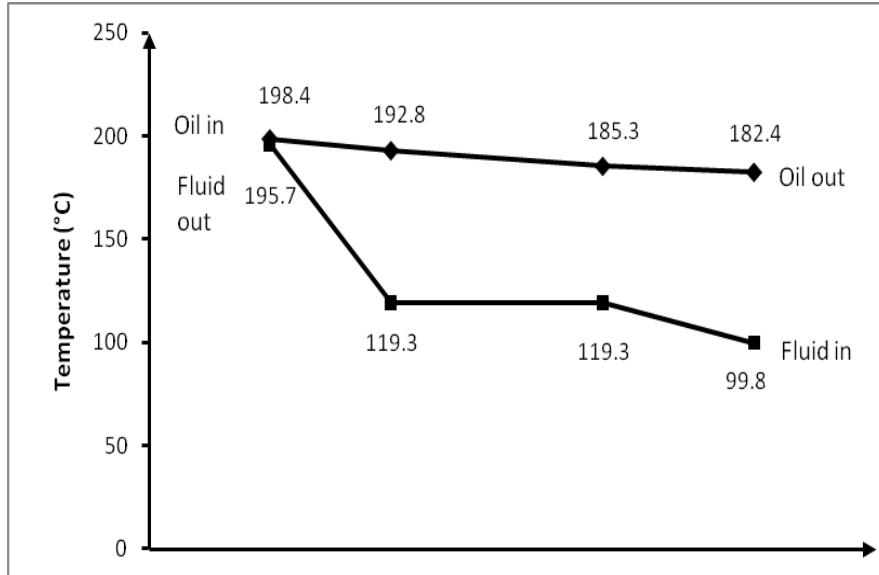
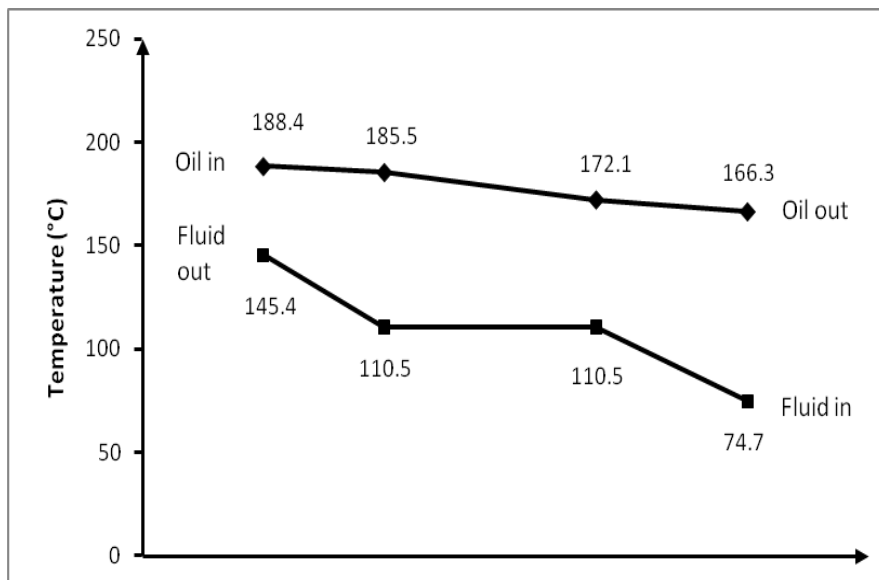Figure 16: Schematics of oil and fluid temperature profiles in the microchannel boiler

Figure 17: Schematics of oil and fluid temperature profiles in the plate boiler

The influence of recuperator effectiveness on ORC cycle efficiencies and overall system COP is shown in Fig. 18. The trends for both efficiency and COP show a linear behavior, indicating 10% of improvement for both the 1st and 2nd law efficiencies when using the microchannel recuperator. The linear improvement of the system COP is directly tied to the 1st law efficiency of the ORC. The primary reason for improved 1st law efficiency with higher recuperator performance was explained above, which is due to reduced heat input from the boiler for the same amount of power output. The improvement of 2nd law efficiency, on the other hand, is attributed to less exergy destruction in the recuperator.
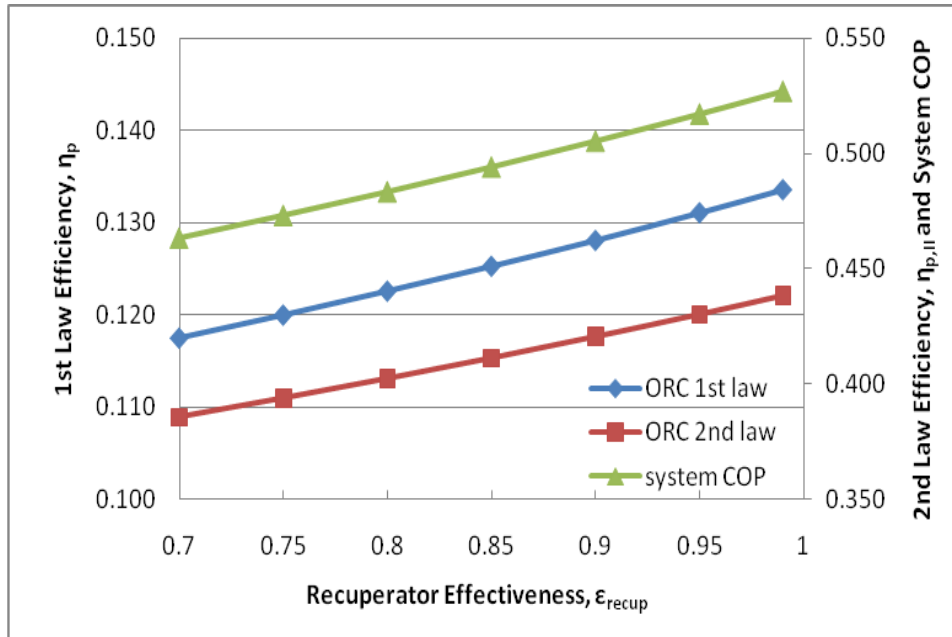
Figure 18: Model data to show the effect of recuperator effectiveness on cycle performance (the plate recuperator effectiveness = 82% while the microchannel recuperator effectiveness > 98%)

5   Conclusions

A novel thermally activated cooling system, using microchannel heat transfer components and combing an ORC with a vapor compression cycle, was presented in this paper with the focus on component performance enhancement. The system can be used to recover and convert waste heat directly into cooling. Based on laboratory testing using a hot oil circulating loop as the heat input, the system has operated at steady state conditions and delivered up to 5 kW of cooling. The highest overall system COP achieved during experiments was 0.8. In comparison to the plate case, the microchannel boiler/recuperator operated at higher superheat at the boiler outlet and achieved higher heat transfer effectiveness in the integrated recuperator. This can be directly attributed to the enhanced heat transfer coefficient and additional wetted surface associated with the microchannel configuration. The data justifies the importance of using microchannel heat exchangers to boost overall system performance, especially for portable or mobile applications. The simplified design model, although being conservative, captures the important trend of increasing average heat transfer coefficient of the microchannel recuperator well. When all channel side walls are taking into account as active heat transfer area, the average heat transfer coefficients predicted by the model match the measured ones closely. This also validated the current simplified design approach for microchannel heat exchangers without using the more sophisticated conjugate heat transfer models.

Acknowledgements

References

[1] T.C. Hung, T.Y. Shai, and S.K. Wang, "A review of organic rankine cycles (ORCs) for the recovery of low-grade waste heat," *Energy*, vol. 22, Jul. 1997, pp. 661-667.

[2] E.W. Miller, T.J. Hendricks, and R.B. Peterson, "Modeling Energy Recovery Using Thermoelectric Conversion Integrated with an Organic Rankine Bottoming Cycle," *Journal of Electronic Materials*, vol. 38, 2009, pp. 1206-1213.

[3] Miller, E., T. Hendricks, H. Wang and R. Peterson, "Integrated Dual Cycle Energy Recovery Using Thermoelectric Conversion and an Organic Rankine Bottoming Cycle," *Journal of Power and Energy*, vol. 225, 2010, pp. 33-43.

[4] • Hendricks, T.J., Karri, N.K., Hogan, T.P., D'Angelo, J., Wu, C. Case, E.D., Ren, F., Morrison, A.Q., Cauchy, C.J.,, "Advanced Soldier-Based Thermoelectric Power Systems Using Battlefield Heat Sources," *Proceedings of the Materials Research Society 2009 Fall Meeting*, Boston, MA: 2009.

[5] • Hendricks, T.J., Karri, N.K., Hogan, T.P., and Cauchy, C.J., "New Thermoelectric Materials and New System-Level Perspectives Using Battlefield Heat Sources for Battery Recharging," *Proceedings of the 44th Power Sources Conference*, 2010, pp. 609-612.

[6] M. Kane, "Small hybrid solar power system," *Energy*, vol. 28, 2003, pp. 1427-1443.

[7] G. Pei, J. Li, and J. Ji, "Analysis of low temperature solar thermal electric generation using regenerative Organic Rankine Cycle," *Applied Thermal Engineering*, vol. 30, 2010, pp. 998-1004.

[8] B.F. Tchanche, G. Papadakis, G. Lambrinos, and A. Frangoudakis, "Fluid selection for a low-temperature solar organic Rankine cycle," *Applied Thermal Engineering*, vol. 29, 2009, pp. 2468-2476.

[9] H. Madhawahettiarachchi, M. Golubovic, W. Worek, and Y. Ikegami, "Optimum design criteria for an Organic Rankine cycle using low-temperature geothermal heat sources," *Energy*, vol. 32, 2007, pp. 1698-1706.

[10] F. Heberle and D. Brüggemann, "Exergy based fluid selection for a geothermal Organic Rankine Cycle for combined heat and power generation," *Applied Thermal Engineering*, vol. 30, 2010, pp. 1326-1332.

[11] K.K. Srinivasan, P.J. Mago, and S.R. Krishnan, "Analysis of exhaust waste heat recovery from a dual fuel low temperature combustion engine using an Organic Rankine Cycle," *Energy*, vol. 35, 2010, pp. 2387-2399.

[12] D. Wei, X. Lu, Z. Lu, and J. Gu, "Dynamic modeling and simulation of an Organic Rankine Cycle (ORC) system for waste heat recovery," *Applied Thermal Engineering*, vol. 28, 2008, pp. 1216-1224.

[13] S. Quoilin, V. Lemort, and J. Lebrun, "Experimental study and modeling of an Organic Rankine Cycle using scroll expander," *Applied Energy*, vol. 87, 2010, pp. 1260-1268.

[14] Y. Dai, J. Wang, and L. Gao, "Parametric optimization and comparative study of organic Rankine cycle (ORC) for low grade waste heat recovery," *Energy Conversion and Management*, vol. 50, 2009, pp. 576-582.

[15] J. Roy, M. Mishra, and A. Misra, "Parametric optimization and performance analysis of a waste heat recovery system using Organic Rankine Cycle," *Energy*, 2010.

[16] D. Wei, X. Lu, Z. Lu, and J. Gu, "Performance analysis and optimization of organic Rankine cycle (ORC) for waste heat recovery," *Energy Conversion and Management*, vol. 48, 2007, pp. 1113-1119.

[17] T. Hung, "Waste heat recovery of organic Rankine cycle using dry fluids," *Energy*

Conversion and Management, vol. 42, 2001, pp. 539-553.

[18] H. Wang, R.B. Peterson, and T. Herron, "Experimental performance of a compliant scroll expander for an organic Rankine cycle," *Proceedings of the Institution of Mechanical Engineers, Part A: Journal of Power and Energy*, vol. 223, 2009, pp. 863-872.

[19] R.B. Peterson, H. Wang, and T. Herron, "Performance of a small-scale regenerative Rankine power cycle employing a scroll expander," *Proceedings of the Institution of Mechanical Engineers, Part A: Journal of Power and Energy*, vol. 222, 2008, pp. 271-282.

[20] J. Bruno, J. Lopezvillada, E. Letelier, S. Romera, and A. Coronas, "Modelling and optimisation of solar organic rankine cycle engines for reverse osmosis desalination," *Applied Thermal Engineering*, vol. 28, 2008, pp. 2212-2226.

[21] G. Kosmadakis, D. Manolakos, S. Kyritsis, and G. Papadakis, "Economic assessment of a two-stage solar organic Rankine cycle for reverse osmosis desalination," *Renewable Energy*, vol. 34, 2009, pp. 1579-1586.

[22] D. Manolakos, G. Kosmadakis, S. Kyritsis, and G. Papadakis, "Identification of behaviour and evaluation of performance of small scale, low-temperature Organic Rankine Cycle system coupled with a RO desalination unit," *Energy*, vol. 34, 2009, pp. 767-774.

[23] D. Tuckerman and R. Pease, "High performance heat sinking for VLSI," *IEEE Electronic Device Letter*, vol. 2, 1981, pp. 126-129.

[24] P. Lee, S.V. Garimella, and D. Liu, "Investigation of heat transfer in rectangular microchannels," *International Journal of Heat and Mass Transfer*, vol. 48, Apr. 2005, pp. 1688-1704.

[25] P. Lee and S.V. Garimella, "Thermally developing flow and heat transfer in rectangular microchannels of different aspect ratios," *International Journal of Heat and Mass Transfer*, vol. 49, Aug. 2006, pp. 3060-3067.

[26] W. Owhaib, "Experimental investigation of single-phase convective heat transfer in circular microchannels," *Experimental Thermal and Fluid Science*, vol. 28, 2004, pp. 105-110.

[27] M.E. Steinke and S.G. Kandlikar, "Single-phase liquid friction factors in microchannels," *International Journal of Thermal Sciences*, vol. 45, Nov. 2006, pp. 1073-1083.

[28] H.S. Park and J. Punch, "Friction factor and heat transfer in multiple microchannels with uniform flow distribution," *International Journal of Heat and Mass Transfer*, vol. 51, Aug. 2008, pp. 4535-4543.

[29] N. García-Hernando, A. Acosta-Iborra, U. Ruiz-Rivas, and M. Izquierdo, "Experimental investigation of fluid flow and heat transfer in a single-phase liquid flow micro-heat exchanger," *International Journal of Heat and Mass Transfer*, vol. 52, Nov. 2009, pp. 5433-5446.

[30] G. Gamrat, M. Favre-Marinet, and D. Asendrych, "Conduction and entrance effects on laminar liquid flow and heat transfer in rectangular microchannels," *International Journal of Heat and Mass Transfer*, vol. 48, Jul. 2005, pp. 2943-2954.

[31] P. Rosa, T. Karayiannis, and M. Collins, "Single-phase heat transfer in microchannels: The importance of scaling effects," *Applied Thermal Engineering*, vol. 29, 2009, pp. 3447-3468.

[32] C. Nonino, S. Savino, S. Del Giudice, and L. Mansutti, "Conjugate forced convection and heat conduction in circular microchannels," *International Journal of Heat and Fluid Flow*, vol. 30, Oct. 2009, pp. 823-830.

[33] S. Kandlikar, "A Roadmap for Implementing Minichannels in Refrigeration and Air-Conditioning Systems - Current Status and Future Directions," *Heat Transfer Engineering*,

vol. 28, 2007, pp. 973-985.

[34] C.Y. Park and P. Hrnjak, "Experimental and numerical study on microchannel and round-tube condensers in a R410A residential air-conditioning system," *International Journal of Refrigeration*, vol. 31, Aug. 2008, pp. 822-831.

[35] Z. Qi, Y. Zhao, and J. Chen, "Performance enhancement study of mobile air conditioning system using microchannel heat exchangers," *International Journal of Refrigeration*, vol. 33, 2010, pp. 301-312.

[36] L. Shao, L. Yang, and C. Zhang, "Comparison of heat pump performance using fin-and-tube and microchannel heat exchangers under frost conditions," *Applied Energy*, vol. 87, 2010, pp. 1187-1197.

[37] P. Hrnjak and A. Litch, "Microchannel heat exchangers for charge minimization in air-cooled ammonia condensers and chillers," *International Journal of Refrigeration*, vol. 31, 2008, pp. 658-668.

[38] S.G. Kandlikar, "Fundamental issues related to flow boiling in minichannels and microchannels," *Experimental Thermal and Fluid Science*, vol. 26, Jun. 2002, pp. 389-407.

[39] H. Wang, R. Peterson, K. Harada, E. Miller, R. Ingram-Goble, L. Fisher, J. Yih, and C. Ward, "Performance of a combined organic Rankine cycle and vapor compression cycle for heat activated cooling," *Energy*, vol. 36, Jan. 2011, pp. 447-458.

[40] F. Incropera and D. Dewitt, *Fundamentals of Heat and Mass Transfer*, Hoboken: Wiley, 2007.

[41] G. Morini, "Scaling effects for liquid flows in microchannels," *Heat Transfer Engineering*, vol. 27, 2006, pp. 64-73.

[42] G. Maranzana, I. Perry, and D. Maillet, "Mini- and micro-channels: influence of axial conduction in the walls," *International Journal of Heat and Mass Transfer*, vol. 47, Aug. 2004, pp. 3993-4004.

[43] P. Hrnjak and A.D. Litch, "Microchannel heat exchangers for charge minimization in air-cooled ammonia condensers and chillers," *International Journal of Refrigeration*, vol. 31, Jun. 2008, pp. 658-668.

[44] C.Y. Park and P. Hrnjak, "Experimental and numerical study on microchannel and round-tube condensers in a R410A residential air-conditioning system," *International Journal of Refrigeration*, vol. 31, Aug. 2008, pp. 822-831.